J. Membrane Biol. 189, 105–118 (2002)
DOI: 10.1007/s00232-002-1011-y

The Journal of
Membrane
Biology



# A New Level Detector for Ion Channel Analysis

**T. Riessner[1], F. Woelk[1], M. Abshagen-Keunecke[1], A. Caliebe[2], U.-P. Hansen[1]**
[1]Center of Biochemistry and Molecular Biology of the Christian-Albrechts-Universität, Leibnizstr. 11, 24098 Kiel, Germany
[2]Mathematical Seminar, Ludewig-Meyn-Str. 4, 24098 Kiel, Germany

Received: 22 January 2002/Revised: 10 June 2002

**Abstract.** The algorithm proposed here for automatic level detection in noisy time series of patch-clamp current is based on the detection of jump-free sections in the time series. The detector moves along the time series and uses a $\chi^2$ test for the detection of jumps. When a jump is detected, the mean value, the variance and the length of the preceding jump-free section are stored. A Student's *t*-test was employed for the assignment of detected jump-free sections to discrete levels of the Markov model and for rejection of all sections with multiple assignments.

The choice of the two significance levels is based on a 3-D diagram displaying the average number of detected levels from several time series *vs.* the significance levels of jump detection and of level assignment. The correct one is selected out of several plateaus with integer number of levels by means of the criterion of minimum scatter or other plausibility considerations.

The test has been applied to simulated data obtained from a 2-state model and a 5-state aggregated Markov model, and the influences of SNR and of gating frequency are shown. Finally, the performance of the level detector is compared with a fit-by-eye and with a fit of the amplitude histogram by a sum of gaussians. At high noise, the fit of amplitude histograms failed, whereas the other two approaches were about equal.

**Key words:** (Aggregated) Markov model — Anti-aliasing filter — Channels — Level detection — Patch clamp — Time series

## Introduction

The kinetic behavior of ion channels is described by Markov processes (Korn & Horn, 1988; Yeo et al., 1988, Ball & Rice, 1992). There exist three main approaches for evaluating the model associated with a time series of measurements of patch-clamp current: one- or two-dimensional dwell-time analysis (Magleby & Weiss, 1990; Magleby & Song, 1992; Colquhoun, Hawkes & Srodzinski, 1996; Blunck et al., 1998), direct fit of the time series (Fredkin & Rice, 1992; Albertsen & Hansen, 1994; Klein, Timmer & Honerkamp, 1997; Farokhi, Keunecke & Hansen, 2000) or analysis of beta distributions (FitzHugh, 1983; Yellen, 1984; Klieber & Gradmann, 1993; Riessner, 1998).

The first two methods require the a priori knowledge of the symbols of the Markov process, i.e., the original current levels related to distinct conductivity states of the investigated channel(s). In the case of dwell-time analysis, the current levels have to be known in order to set the threshold values of the jump detectors (Schultze & Draber, 1993; Draber & Schultze, 1994; Hansen et al., 1995). For the direct fit of the time series, a predicted current level is compared with the measured one. Thus, the original levels of the channel(s) have to be known before the analysis starts. However, in real records, the time series are heavily corrupted by noise, and it is very difficult to find the original current levels. Often, an amplitude histogram is created from the measured record and the original levels are determined as the centers of the gaussian distributions used to fit the measured amplitude histogram. This works fine as long as the "valleys" between individual distributions are not filled up by noise.

Here, a novel level detector is described consisting of two test procedures. The first one, based on a $\chi^2$ criterion, seeks to find jump-free time sections in a noisy time series, even if the signal-to-noise ratio (SNR) is poor (down to 0.25). For other approaches that deal with the problem of detecting a change in parameters (i.e., a jump of the current level), *see*, e.g., the literature on AMOC renewal processes

*Correspondence to:* U.-P. Hansen; email: uphansen@zbm.uni-kiel.de

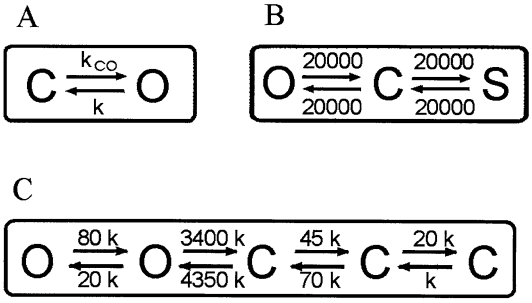


**Fig. 1.** Three models used for testing the level detector. (*A*) Two-state Markov model, (*B*) Three-state Markov model, and (*C*) Five-state aggregated Markov model. The factor $k$, the scaling factor for the rate constants, is used on the abscissa in Figs. 7, 8, 9 and 10, below.

(Horvàth & Steinebach, 2000; Hušková & Steinebach, 2000) or on maximum likelihood ratio tests (Horváth, 1993). The second test assigns the jump-free sections to putative current levels of the ion channel.

## Methods

Markov models of ion channels were used for the generation of time series to test the algorithms. A Markov model is the generally accepted presentation of the gating behavior of a channel (Konn & Horn, 1988). It consists of different states, mostly called O (open), S (sublevel), and C (closed). The actual state of the channel is assigned to one state of this Markov model. Transitions from one state to the other occur spontaneously with rate constants $k_{ij}$ (or transition probabilities $p_{ij}$) as depicted in Fig. 1. If the conductance levels (symbols $S_j$) are not different for all states, the model is called an aggregated Markov model (Ball et al., 1993).

For the illustration of the operation and the problems of the level detector three models are used: a simple 2-state Markov model (Fig. 1*A*, C-O), a 3-state Markov sublevel model (Fig. 1*B*, O-C-S), and a 5-state aggregated Markov model (Fig. 1*C*, O-O-C-C-C, Farokhi et al., 2000). The C-O model is often used when a new algorithm for data analysis is presented (FitzHugh, 1983; Crouzy & Sigworth, 1990).

Simulations of time series related to a given (aggregated) Markov model were done by the following routine. It started with the selection of a state of the Markov model. In order to get a stationary Markov time series, the range between 0 and 1 was divided into sections proportional to the steady-state concentrations of the Markov states. Then, a uniformly distributed random number between 0 and 1 was generated, and that state was selected in whose section the random number fell. This state was the source state $R_r$ for the first jump. For this jump, the random generator delivered two other uniformly distributed numbers. The first one ($n_1$) was used to calculate the time of the next jump from the source state $R_r$ to the sink (destination) state $R_S$ (continuous time). The dwell-time distribution of the source state $R_r$ is

$$R_r(k) = 1 \cdot \exp(-\lambda_r k\Delta t) \quad \text{with} \quad -K_{rr} = \lambda_r = \sum_{s\neq r} k_{rs} \tag{1}$$

s labels all possible sink states for a jump out of the present state $R_r$. The first random number $n_1$ was used as an entry of the ordinate of Eq. 1 (i.e., as a value of $R_r$), and the related value $k\Delta t$ at the abscissa was taken as the time of the jump (Press et al., 1987). The amplitude factor "1" in Eq. 1 was used because the random number $n_1$ is uniformly distributed between 0 and 1:

$$k\Delta t = -\frac{1}{\sum_{s\neq r} k_{rs}} \ln(n_1) \tag{2}$$

Now, the second random number $n_2$ (uniformly distributed, $0 \le n_2 \le 1$) gave the aim (sink state $R_S$) of the jump. The section between 0 and 1 was divided into sections of length $k_{rs}/\lambda_r$ assigned to the states $R_S$ as described above for the starting state. The state $R_S$, in whose section $n_2$ happened to fall, was called the sink (destination) state. The system still remained in state $R_r$ for the time $t_k = k\Delta t$ (Eq. 1). Then, the jump to $R_S$ occurred, and after this jump, the algorithm started again from this new state by generating two new random numbers.

The effect of the anti-aliasing filter was introduced as follows: The jump caused a response of the 4-pole Bessel anti-aliasing filter, which was taken out of a memory. In this memory, the theoretically determined jump responses of the different anti-aliasing filters were stored. Thus, the series of jumps $I(t)$ created by the random generators resulted in a sum of delayed filter responses, i.e., the measured current

$$I(t) = \sum_{k=j_1}^{j} I_{rs,k}\ h(t - t_k) \tag{3a}$$

with

$$t_k = \sum_{i=1}^{k} \Delta t_i \quad \text{and} \quad h(t) = 0 \quad \text{for} \quad t < 0 \tag{3b,c}$$

with $I_{rs,k}$ being the step in current related to the jump from state $R_r$ to $R_S$ at time $t_k$. $t_k$ was given in continuous time (Eq. 2), and mostly did not coincide with the sampling points. Then, $h(t-t_k)$ was obtained from interpolation of the stored values of the stored step responses of the anti-aliasing filter $h(t)$. The lower limit $j_1$ of the sum in Eq. 3 was determined by the fact that those responses could be omitted if the related $1-h(t)$ had decreased below one bit of the DA converter.

This procedure resulted in a much shorter computing time for the calculation of a time series of 2,000,000 samples than an algorithm making a decision at every sampling point if and where to jump. In addition, this program generated a continuous Markov process, as natural channels do. It automatically included multiple jumps in a sampling period $T_S$.

Then, the generated time series was superimposed by noise. White gaussian noise was generated by a Box-Muller algorithm (Press et al., 1987). Filtering to obtain white, red or blue noise could be done by digital filtering. In the simulations, red noise (prefiltered by the same filter $h(t)$ as used in Eq. 3 was used. As always the same time course of the noise was used in the simulations, (variations occurred only in the time series of the "channel"), the whole time series of noise was stored in the computer. For composing a surrogate noisy patch-clamp record, the freshly prepared time series of the Markov process was added to the stored noise series with the same anti-aliasing filter. The signal-to-noise ratio was defined by

$$\text{SNR} = \left(\frac{\Delta I}{\sigma_b}\right)^2 \tag{4}$$

with $\Delta I$ being the average difference in the currents of the related levels and $\sigma_b$ the standard deviation of the background noise. The assumed sampling rate was 200 kHz, and the anti-aliasing filter was a 4-pole Bessel filter with a corner frequency of 50 kHz.

## Abbreviations

| | |
|---|---|
| $A(I)$, | amplitude histogram of measured current; |
| $F_S$, | significance level for splitting of the time series into jump-free intervals; |
| $F_1(t)$, | distribution function of the Student's $t$-test; |
| $I$, | current; |
| $\bar{I}$, | mean current; |
| $I_k$, | sampled value of the current at time k; |
| $I_{bk}$, | sampled value of background noise at time k; |
| $I_S$, | jump in current as caused by a transition between states; |
| $L_t$, | significance level for the Student's $t$-test for the probability that two samples have the same mean; |
| $k_{ij}$, | rate constants of transition between the states of a Markov model; |
| $m$, | number of levels; |
| $m_E$, | number of detected levels; |
| $m_M$, | number of levels of Markov model; |
| $n_e$, | number of excluded data points; |
| $n_r$, | reduced length of detected jump-free section; |
| $n_0$, | mean of reduced length of apparent jump-free sections; |
| $R_r$, | source state of Markov model; |
| $R_S$, | sink (destination) state of the Markov model; |
| $\bar{S}_i$, | mean value of detected markov level $i$; |
| $\bar{S}_{ij}$, | mean value of the j$^{th}$ jump-free section assigned to Markov level $S_i$ |
| $S_i$, | real Markov level; |
| SNR, | signal-to-noise ratio; |
| $t_j$, | time of a jump; |
| $T_S$, | sampling period; |
| $t_T$, | threshold of the Student's $t$-test; |
| $\Delta t$, | time between jumps; |
| $\Delta_{rel}$, | relative error of the determination of the values of the level in %; |
| $\sigma_b^2$, | standard deviation of the background noise; |
| $\sigma_{bn}^2$, | standard deviation of the background noise from a filtered time series of length $n$; |
| $\sigma_{sn}^2$, | standard deviation of subsections of the time series of length $n$; |
| $\sigma_{S_i}^2$, | scatter of the level $S_i$; |
| $\sigma_\sigma$, | Scatter of the scatter of the assumed levels; |
| $\chi_{n-1}^2$, | $\chi^2$ distribution for jump detection in subsections of length $n$ |

## Theory of the New Level Detector

The new algorithm comprises several steps:

- elimination of linear drift and hum due to the AC power source (optional, if necessary)
- determination of the standard deviation of the background noise $\sigma_b$ from a jump-free time series of the same or an equivalent patch. However, after developing the algorithm, a procedure (Fig. 5 below) is provided that does not need the a priori knowledge of $\sigma_b$.
- use of this knowledge for dividing the time series into jump-free subsections
- estimation of the symbols of the Markov model (e.g., current levels) from these subsections
- repetition of the analysis with different significance levels
- selection of the most probable solution (Fig. 5)

The first step making use of common drift elimination procedures (Bendat & Piersol, 1971; Press et al., 1987) is not considered here. A serious problem is the determination of the standard deviation $\sigma_b$ of the jump-free time series. One method is to block the channel(s) by an inhibitor to get $\sigma_b$ from the resulting time series. Here, we start from the assumption that $\sigma_b$ is known. Later on (Fig. 5), it is shown that the a priori knowledge of $\sigma_b$ is of minor importance.

### Detection of Jump-Free Sections

Cutting the time series into subsections without jumps is based on the expectation that a subsection of the time series that contains a jump has a higher standard deviation $\sigma$ than a subsection without a jump. This leads to the following procedure: If $\sigma$ exceeds an adequate threshold, it is assumed that a jump has occurred. Because of the statistical nature of the noise, it may happen that jumps remain undetected for some values of the threshold. However, before dealing with this problem, the procedure for jump detection is described.

The threshold for the standard deviation, $\sigma_{sn}$, depends on the length $n$ of the subsection and on the standard deviation of the background noise $\sigma_b$. For the numerical decision of whether a time series with $n$ data points $I_i$, contains a jump, $X_{n-1}^2$ is calculated

$$X_{n-1}^2 = \sigma_{bn}^2 \chi_{n-1}^2 = (n-1)\sigma_{sn}^2 = \sum_{i=1}^{n} (I_i - \bar{I})^2 \qquad (5)$$

$\bar{I}$ in Eq. 5, is the mean value of the current of the inspected section. In a real patch-clamp setup, the anti-aliasing filter causes an internal correlation of the noise. The resulting deviation from normal distributed data implies that the significance levels become different from $F_S$ in Eq. 7. Especially, the variance of the noise $\sigma_b$ is not independent of the length $n$ of the section. As an attempt to account for this problem, $\sigma_{bn}$ was determined from a jump-free section of the time series of length $n$ and was stored on the computer for the evaluation by means of Eqs. 6 and 7.

The distribution function of the $\chi_{n-1}^2$ value of $n$ normal-distributed variables $I_i$ of the noise in a jump-free section with standard deviation $\sigma_{bn}$ is (Kreyszig, 1982)

$$F_1(\chi_{n-1}^2) = \frac{1}{2^{\frac{n}{2}}\Gamma(\frac{n}{2})} \int_0^{\chi_{n-1}^2} u^{n-2} \exp\left(-\frac{u}{2}\right) du = P\left(\frac{n}{2}, \frac{X_{n-1}^2}{\sigma_{bn}^2}\right) \qquad (6a)$$

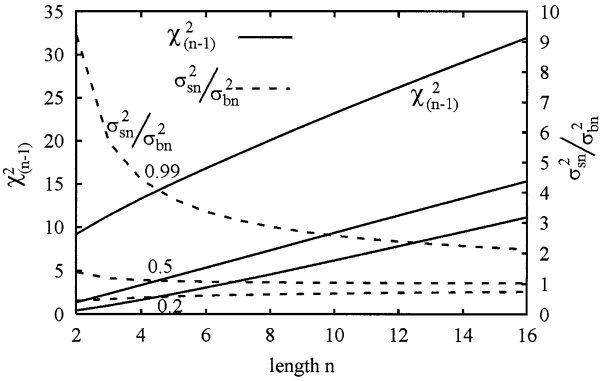


**Fig. 2.** Confidence interval $[0, \chi^2_{n-1,u}]$ (range of legitimate $\chi^2_{n-1}$-values and of relative scatter, $\sigma_{sn}/\sigma_{bn}$ (Eq. 5) of the signal in the section of $n$ at given $F_S$; index $u$ gives upper limit) calculated from Eqs. 6 and 7 are shown for three different significance levels ($F_S$ = 0.99, 0.5, 0.2, as indicated in the figure) for interval lengths ($2 \le n \le 16$).

with $P$ being the incomplete gamma function

$$P(a,x) = \frac{1}{\sqrt{a}} \int_0^x e^{-t} t^{a-1} dt \qquad (6b)$$

Because of Eq. 5, this distribution function for jump-free sections does not depend on the mean $\bar{I}$ (i.e., on the actual symbol of the Markov model) of the random variables $I_i$. A significance level $F_S$ is chosen, and the upper limit of the $X^2_{n-1}$-value or the related $\sigma_{sn}$ (Fig. 2) is calculated as follows

$$F_S = F_I\left(\frac{X^2_{n-1}}{\sigma^2_{bn}}\right) = F_I(\chi^2_{n-1}) \qquad (7)$$

For the calculation of $X^2_{n-1}$ (or $\sigma_{sn}$, Eq. 5) from Eqs. 6a and 7, the numerical implementation of the incomplete gamma function $P$ (Eq. 6b) as given by Press et al. (1987) is used.

Figure 2 shows the dependence of the confidence interval on the length $n$ of the subsection of the time series for different significance levels $F_S$. For instance $F_S = 0.9$ means that 10% of the detected jumps were false alarms. The shorter the subsection, the greater is the range of tolerable $\sigma^2_{sn}$-values for reasonable confidence levels. Because of this statistical uncertainty in short sections, small jumps may be hidden in the variance of the $\sigma^2_{sn}$-value. The tolerance interval gets narrower in long subsections. Thus, even small jumps that cause just a small increase of the $\sigma_{sn}$-value can be detected in a long subsection.

Analysis of measured time series is based on the inspection of sections of the time series $I_i$ of different length $n$. $n$ is an integer power of 2 in order to increase calculation speed. The time series of Fig. 3*B* (generated by the Markov model in Fig. 3*A* and shown for SNR = 4) is used to demonstrate the operation of the jump detector. The test section of length $n$ moves along the time series. At each point $t_k$ of the time series, the $X^2_{n-1}$ value of the section from $t_{k-n+1}$ to $t_k$ is calculated (Eq. 5) and plotted versus time. The run starts with $n = 2$ (Fig. 3*C*, *E*, *G*). Then, the procedure is repeated with $n = 4$, 8, and 16. The results obtained for $n = 16$ are shown in Fig. 3*D*, *F*, and *H*.

Figure 3 shows the influence of the length $n$ of the inspected interval, the length of the event, the significance level $F_S$ (Eq. 7) and signal-to-noise ratio (SNR, Eq. 4). The example for nearly noise-free records (SNR = 400) shows the benefit of short sections, namely high temporal resolution. With $n = 2$, all jumps are clearly indicated (Fig. 3*C*), whereas $n = 16$ is too long (as in Fig. 3*F* and *H*), and fails to detect the jump-free section between the jumps of the short event. This is not a serious problem, as discarding a section is always on the safe side.

The comparison of Fig. 3*G* and Fig. 3*H* demonstrates the influence of the length of the inspected interval at very high noise (SNR = 1). In Fig. 3*G* ($n = 2$), the high $\sigma_{bn}$ causes such a broad confidence interval (Eq. 7, Fig. 2) that the significance level $F_S = 0.95$ is reached only once. According to Eq. 8 below, $n = 16$ yields a better chance to reach $F_S = 0.95$ in the case of the long event. For $F_S = 0.9$, not all peaks at $n = 2$ in Fig. 3*G* (and also in Fig. 3*E*) can be assigned to true jumps, as their occurrence is not related to the position of the jumps. Thus, there exists no adequate significance level for $n = 2$. In the case of $n = 16$, a significance level of 0.95 leads to the detection of the jumps of the long event, whereas in the case of the short event (4 data points) the long section (19 data points) averages over open and closed events, and thus decreases $X^2$. At SNR = 4, $n = 2$ fails again. With $n = 16$, the long event is detected with high reliability. The section with the short event is excluded at $F_S = 0.7$. Discarding parts of the time series (as in the case of the short event with adequate significance levels in Fig. 3*D*, *F*, *H*) may not be a major problem, as the statistics of dwell times (Eq. 1) imply that a longer event with the same current level will occur somewhere else in the time series if it is long enough. A serious problem is the inclusion of an undetected jump in an apparently jump-free section, as happens in Fig. 3*E* and *G*. An important message of Fig. 3 is also that the choice of the adequate significance level is crucial for the correct operation. A way to approach this problem is presented below (Fig. 5).

The jump in the middle of the section and the increase of chance of its detection with the length $n$ of the section is obtained from the following considerations. If the jump of magnitude $I_S$ is from low to high current and occurs after $m$ data points in an interval of length $n$ (and does not jump back before $n$), then the mean value $\bar{I}$ of the whole section is $(n-m)/n\ I_S$ above the lower current level, and the expected $X^2_{n-1}$ (related to $\sigma_{sn}$ by Eq. 5) is

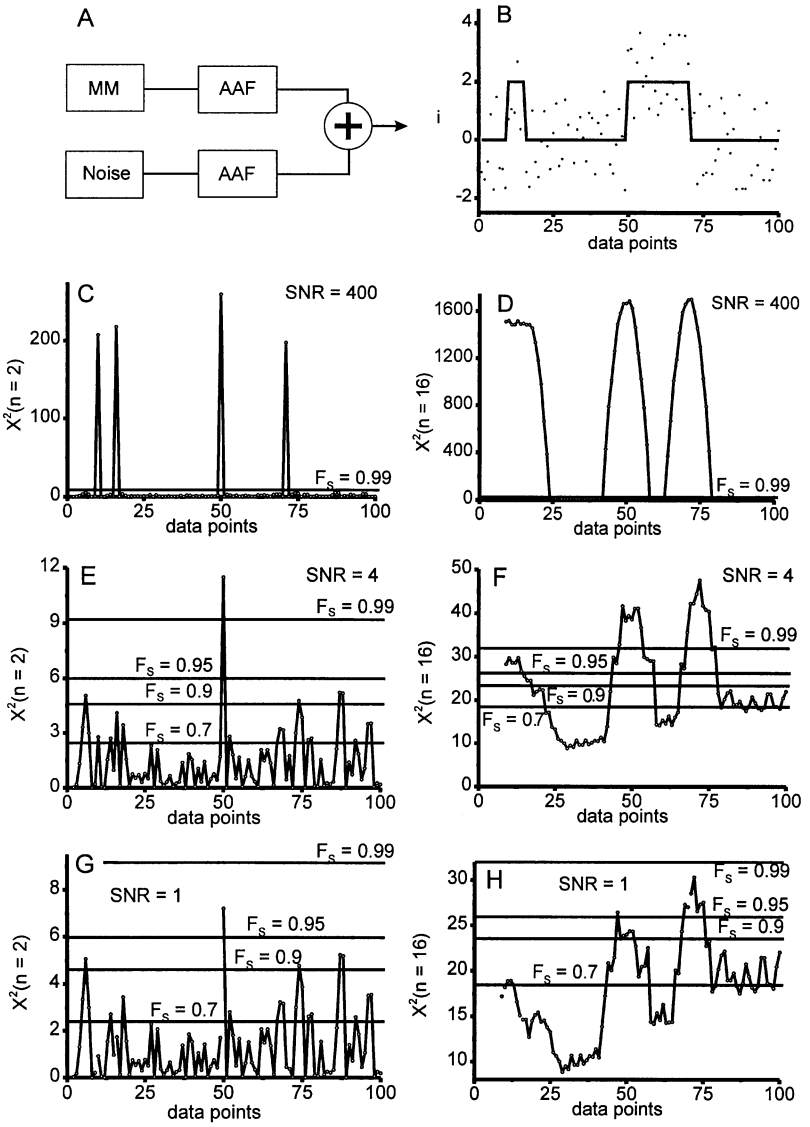


**Fig. 3.** Illustration of the operation and of the parameter dependence of jump detection. The simulated time series were generated as shown in (*A*) but (for the sake of clarity) without anti-aliasing filter (AAF). The unit of the time axis is sampling points = 50 μsec. (*B*). The time series used for illustration with a short (4 data points) and a long (19 data points) opening event is shown for SNR = 4. The time courses of the calculated $\chi^2_{n-1}$ values (Eq. 5) are shown for test sections with the lengths $n = 2$ (*C*, *E*, *G*) and with $n = 16$ (*D*, *F*, *H*) and for different signal-to-noise ratios (Eq. 4) SNR = 400 (*C*, *D*); SNR = 4 (*E*, *F*) and SNR = 1 (*G*, *H*). The horizontal lines indicate the thresholds of the standard deviation for $F_S = 0.9$ and $F_S = 0.99$ (Eq. 7).

$$E[X^2_{n-1}] = E\left[\sum_{k=1}^{n}(I_k - \bar{I})^2\right]$$
$$= E\left[\sum_{k=1}^{m}(\bar{I}_R + I_{bk} - \frac{n-m}{n}I_S - \bar{I}_R - \bar{I}_b)^2 + \sum_{k=m+1}^{n}(I_{bk} + \frac{m}{n}I_S - \bar{I}_b)^2\right] \quad (8a)$$

with $I_R$ being the real (noise-free) mean value and $I_b$ the mean value of the noise in the investigated section. Introducing Eq. 5 for the noise signal $I_{bk}$ and calculating the sum of $(I_S)^2$ terms leads to

$$E[X^2_{n-1}] = E[X^2_{n-1,b}] + \frac{mn^2 - m^2n}{n^2}I_S^2 + E\left[\sum_{k=1}^{n} I_{S,k}(I_{bk} - \bar{I}_b)\right] \quad (8b)$$

$$E[X^2_{n-1}] = (n-1)\sigma^2_{bn} + \frac{mn^2 - m^2n}{n^2}I_S^2 \quad (8c)$$

The expected value of the last term in Eq. 8b is zero (as noise and jump are not correlated). The symbol $I_{S,k}$ accounts for factors before $I_S$ in the sums of Eq. 8a.

Equation 8c has two messages: 1. The derivation $d/dm$ of Eq. 8c shows that the deterministic term gets a maximum value $(nI_S^2)/4$ for $m = n/2$, i.e., if the jump occurs in the middle of the interval. 2. The $I_S^2$ term and the expected value of $X^2$ increase linearly over $n$ if $m$ is a fixed ratio of $n$, especially when $m = n/2$. In contrast, the slope of increase of the threshold of $X^2_{n-1}$ in Fig. 2 for a given $F_S$ is much less (in Fig. 2, $X^2_{n-1}$ for $F_S = 0.99$ increases by a factor of 3, whereas $n$ increases by a factor of 8). Thus, the chance of detecting a jump increases with the length of the inspected section.

The increased chance of jump detection with increasing $n$ becomes obvious from a comparison of Fig. 3*G* and Fig. 3*H* (SNR = 1) or Fig. 3*E* and Fig. 3*F* (SNR = 4), as described above.

Construction of the jump-free section with length $n_r$ starts from the detection of the last two subsequent jump positions, as the section between them is supposed to be jump-free. It has to be mentioned that $n$ (used in Fig. 3 for the length of the test section for the jump detection algorithm) is different from the length $n_r$ of what is stored as jump-free section in the computer. As it is better to exclude more data points than necessary rather than including an undetected jump, the section is shortened by $n/5$ on either side. Usually, an anti-aliasing filter smoothes the transitions. In order to account for this effect, additional $n_e$ datapoints (corresponding to the a priori known time needed by the filter to reach steady state) are omitted from the first part of the final section. The mean value of the remaining subsection, its $\chi^2$, and the reduced section length $n_r$ are stored in an array for later use.

## Reconstructing Levels from the Stored Jump-Free Sections

The determination of the symbols of the Markov process (original current levels of the ion channel) was done by two different approaches:

1. Using a Student's $t$-test for extracting the symbols from the mean values of the jump-free sections. Even though the application of the $t$-test requires independent and identically distributed data, the influence of the anti-aliasing filter is ignored, because of the robustness of the test and because the final significance level is determined by the approach related to Fig. 5 below. This method is the most stupid one, but it turned out to be the most effective one.
2. Generating a 3-dimensional histogram with mean value and special length on the $x$- and $y$-axis, respectively, and the frequency $f$ of occurrence on the $z$-axis. The 3-dimensional histogram is fitted with a sum of theoretical distributions of a single level by means of a least-squares fit or a maximum-likelihood fit. Even though this approach seemed to be more sophisticated, it failed, and is not reported here.

The grouping of jump-free sections of the time series with the same mean began from the levels stored in the array obtained from the detection of jump-free subsections.

The mean value of the longest section is taken as the first level without test. Because of its length, its statistical error is expected to be small. Then, the next section (the second longest one) is taken and the Student's $t$-test (Press et al., 1987) is employed to test whether its mean value is equal to that one of the first section. The distribution function is

$$F_t(t) = \frac{\Gamma\left(\frac{N+1}{2}\right)}{\sqrt{N\pi}\,\Gamma\left(\frac{N}{2}\right)} \int_{-\infty}^{t} \frac{du}{\left(1+\frac{u^2}{N}\right)^{\frac{N+1}{2}}} = 1 - B_{\frac{N}{N+t^2}}\left(\frac{N}{2},\frac{1}{2}\right) \tag{9}$$

with $N = N_1 + N_2 - 2$, $N_1 = n_r$ of the new section, $N_2 = n_r$ of the already assigned section (average of the sections already assigned to $S_i$), $B$ = incomplete beta function (Press et al., 1987), and

$$t = \frac{\bar{I} - \bar{S}_i}{S_{Di}} \tag{10}$$

with $\bar{S}_i$ = symbol (mean value) of level i. With $S_{ij}$ being the mean values of the sections assigned to $S_i$, $S_{Di}$ becomes

$$S_{Di} = \sqrt{\frac{\sum_{j=1}^{N_1}(I_j - \bar{I})^2 + \sum_{j=1}^{N_2}(S_{i,j} - \bar{S}_i)^2}{N_1 + N_2 - 2}\left(\frac{1}{N_1} + \frac{1}{N_2}\right)} \tag{11a}$$

or

$$S_{Di} = \sqrt{\frac{\sum_{j=1}^{N_1} I_j^2 - \frac{1}{N_1}\left(\sum_{i=1}^{N_1} I_i\right)^2 + \sum_{j=1}^{N_2} S_{i,j} - \frac{1}{N_2}\left(\sum_{i=1}^{N_2} S_{i,j}\right)^2}{N_1 + N_2 - 2}} \times \sqrt{\left(\frac{1}{N_1} + \frac{1}{N_2}\right)} \tag{11b}$$

The second form (Eq. 11b) is used for the numerical implementation, because it enables a recursive calculation by summarizing the first and second moments of all sections assigned to a symbol $S_i$ in order to compute $S_{Di}$. Again a threshold value of $t(t_T)$ for rejection has to be selected for

$$L_t = 1 - F_t(t_T) = B_{\frac{N}{N+t^2}}\left(\frac{N}{2},\frac{1}{2}\right) \tag{12}$$

For instance, $F_t = 0.9$ means that $L_t = 10\%$ of the levels with apparently different mean still have the same mean. The value of $t$ in Eq. 10 has to be zero for absolutely identical means of the two data sets. With a given threshold $t_T$, three cases may occur:

1. The section cannot be assigned to any of the already detected symbols. A new level has to be introduced.
2. It can be assigned to one and only one level. Then it is merged into the pool of sections already assigned to this level.

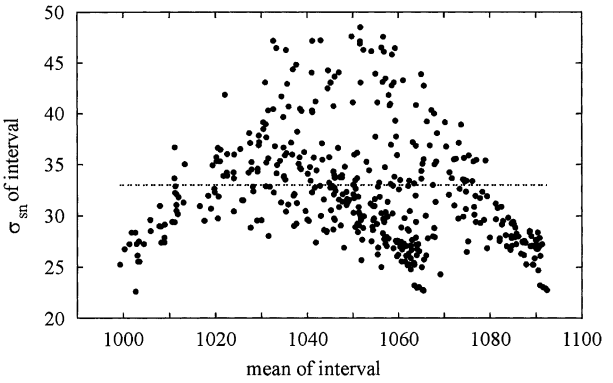


**Fig. 4.** Mean-variance histogram showing the standard deviation $\sigma_{sn}$ *vs.* the mean value of apparent jump-free sections obtained from simulated data generated from a 3-state model O-C-S (Fig. 1) with all rate constants = 20 msec$^{-1}$ and currents O = 1090, S = 1063 and C = 1000, $\sigma_b$ of the jump-free time series was 33 (horizontal dotted line). Only those sections were used whose length was at least 2/3 of the maximum length.

3. It can be assigned to more than one level. It is declined.

After all sections have been inspected, an ensemble of symbols is generated, and the mean and the variance of the symbol (conductance level) $S_i$ can be calculated.

Problems of proper assignment can arise from the fact that in the case of data with poor SNR it may happen that there are apparent jump-free sections, which contain an undetected jump as in Fig. 3*E*, *G* for all confidence levels, in Fig. 3*H* for $F_S = 0.9$ and in Fig. 3*F* for $F_S = 0.99$ in the case of the short event. The inclusion of such undetected jumps would generate new, but false symbols, because their mean is somewhere between two real symbols, and thus cannot be assigned to one of them. Approaches to overcome these problems are mainly based on an adequate choice of the significance levels $F_S$ (Eq. 7) and $L_t$ (Eq. 12).

A problem that cannot be solved by the procedures suggested here is the reduction of apparent levels by the averaging function of the anti-aliasing filter in the case of fast gating (Hansen, Keunecke & Blunck, 1997; Townsend & Horn, 1999). In that case, a direct fit of the time series based on an adequate Hidden-Markov model is required (Farokhi et al. 2000; Zheng, Vankataramanan & Sigworth, 2001).

The scatter of $\sigma_{sn}$ occurring in different sections of a time series is illustrated by means of a mean-variance histogram (Patlak, 1993) constructed from simulated data obtained from a 3-state model O-C-S (Fig. 1) as specified in the legend of Fig. 4. Figure 4 shows that there exist sections with noise quite far below the average of $\sigma_b$ of the noise-free time series. Those sections with the lowest noise come close to the original mean values (symbols of the Markov process).

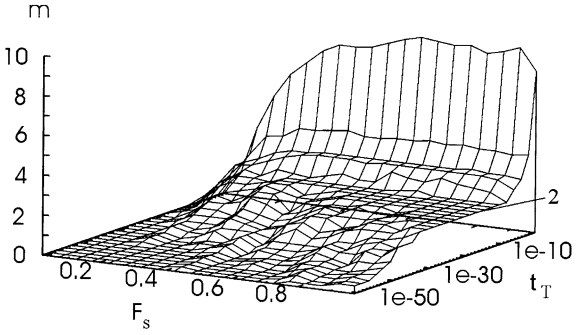


**Fig. 5.** Dependence of the average number of detected levels on significance level $F_S$ and threshold $t_T$. Results from 10 time series simulated on the basis of a symmetrical 2-state model (Fig. 1) with $k_{OC} = k_{CO} = 15$ msec$^{-1}$. The correct number of levels is 2. The low values of $L_t$ result from the incomplete Beta function B (Eq. 12).

It may be argued that plots like Fig. 4 are sufficient for level detection. However, its evaluation still requires human interaction, whereas the level detector developed here is designed to do its job automatically. Nevertheless, Fig. 4 shows that selecting the section with minimum noise gives symbols (levels) close to the real ones.

The influence of both significance levels $F_S$ and $L_t$ (related to the threshold $t_T$) becomes apparent from 3-D plots like that shown in Fig. 5. Here, the average number of detected levels $m$ is plotted over the $F_S$-$t_T$ plane. In the case of real patch-clamp data, the generation of such plots requires several experiments on the same system. The number of experiments can be increased by cutting long records into smaller ones. However, care has to be taken that rare events are not excluded from some of the short records. In Fig. 5, ten time series were simulated with a two-state model with 2 conductance levels (open—closed). Non-integer numbers of $m$ result from averaging over the results from different time series. They are an indication that the choice of $F_S$ and $L_S$ has not been appropriate. A plateau is seen at zero levels (wrong) and 2 levels (correct).

An additional criterion is required if the results are not so convincing as in Fig. 5. Often, several plateaus with an integer number of channels can be observed, and the correct plateau may not be the widest. In that situation, the inspection of the scatter of the scatter, $\sigma_\sigma$, of the levels $S_i$ turned out to be powerful. For this purpose, the variance of each of the detected levels was determined.

$$\sigma_{S_i}^2 = \frac{1}{n_{Ai} - 1} \sum_{k}^{n_{Ai}} (S_i - I_{k,i})^2 \tag{13a}$$

$n_{Ai}$ is the number of all data points of all sections assigned to the level $S_i$, $I_{k,i}$ is the sampled current value assigned to level $S_i$. Then, the scatter of the scatter was calculated

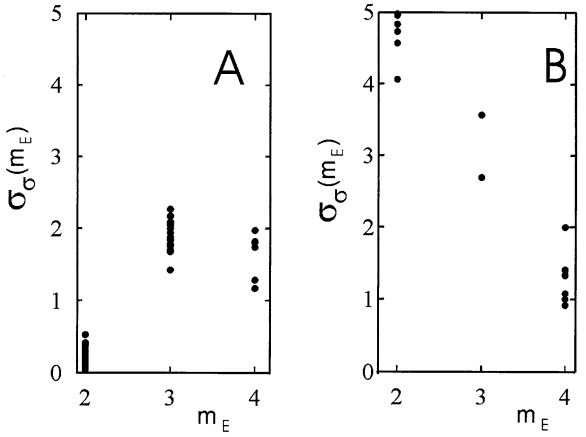


**Fig. 6.** Using the scatter of the scatter of the levels $\sigma_\sigma$ ($m_E$) for determining the most probable number of levels $m_E$. $\sigma_\sigma$ ($m_E$) (Eq. 13) is plotted *vs.* the number of detected levels ($m_E$). (*A*) One 2-state channel with 2 levels. (*B*) Three 2-state channels resulting in 4 levels.

$$\sigma_\sigma^2(m_E) = \frac{1}{m_E}\sum_{i=1}^{m_E}(\sigma_{S_i} - \bar{\sigma}_{S_i})^2 \qquad (13b)$$

$\sigma_\sigma(m_E)$ is expected to be minimum if the number $m_E$ and values of levels are correct. Figure 6 gives two examples. This, however, does not work in the case of strong scatter, when the σ-environments of the levels overlap as shown below (Fig. 12).

## The Output of the Computer Program

For the computer program (www.zbm.uni.kiel.de/software/leveldet.html), two time series are required. The time series with jumps that has to be analyzed, and a jump-free time series. (The last one is not necessarily required, as $F_S$ (Eq. 7) can be obtained from diagrams like Fig. 5, but its knowledge provides a hint to the adequate range). After starting the computer, a list of possible results is delivered according to Fig. 5. A result is a block of data assigned to a number of levels that is related to a plateau in Fig. 5. Each one of these blocks comprises:

- the number $m_E$ of levels assigned to this block
- the size of the area of the related plateau in Fig. 5
- the variance of the variance ($\sigma_\sigma(m_E)$) of related levels according to Fig. 6
- the current values $S_i$ of the detected levels
- the noise $\sigma_{S_i}^2$ of each determined level
- the number of data points contributing to each level
- the number of jump-free sections contributing to each level

In the absence of fast gating, the computer automatically selects the best result from the list by choosing the block with minimal variance of the detected levels or with minimum variance of the variance of the levels. In addition, the complete list of results is shown, in order to leave the final decision to the user. The necessity of this inspection is shown below (evaluation related to Fig. 12).

Criteria for the necessity of a user decision are: very few data points assigned to a level (unreliable level), different scatters of the levels (may indicate fast gating). In these cases, a general recipe cannot be given. Instead, the experience of the user is required.

Short sections may lead to improper assignment. If the first section opening a new level has a strong deviation from its true current, then the selection of the subsequent section assigned to this level is biased. We found that two strategies were successful:

1. Before the analysis is done, the sections are sorted, and the analysis starts with the longest section.
2. A subsection that cannot be assigned to existing levels may only open a new level if its noise is lower than 90% of the noise of the jump-free time series according to Fig. 4.

For a time series with 2 million data points, the time for a run of the level detector on an Athlon 1.4 GHz is about 45 min.

## Testing the Level Detector with Simulated Time Series with Different Gating Frequencies and High and Low SNR

Simulations of time series were done as described in Methods. For the purpose here, a 2-state model may be considered as sufficient, because only the dwell times on a level are important for the detection of this level, and it does not matter whether the system jumps around between aggregated states of equal conductance. Nevertheless, for the asymmetric case, an aggregated Markov model is used, the 5-state model used by Farokhi et al. (2000), to describe the fast gating that causes the AMFE (anomalous mole fraction effect) in *Chara*.

The quality of the results is presented by two criteria. The first one is the finding of the number $m_E$ of correct levels. The second one is the relative error of the determination of the values of the levels

$$\Delta_{rel} = \frac{1}{m_E}\sum_{i=1}^{m_E}\frac{|\bar{S}_i - S_{i,next}|}{\overline{\Delta S}} \qquad (14)$$

with $m_E$ being the number of experimentally determined current levels in the assumed (aggregated) Markov model, $\overline{\Delta S}$ the average distance between the Markov states, $S_i$, the symbol (current value) determined by the level detector and $S_{i,next}$, the real Markov state (known from the simulations) that is closest to $\bar{S}_i$.

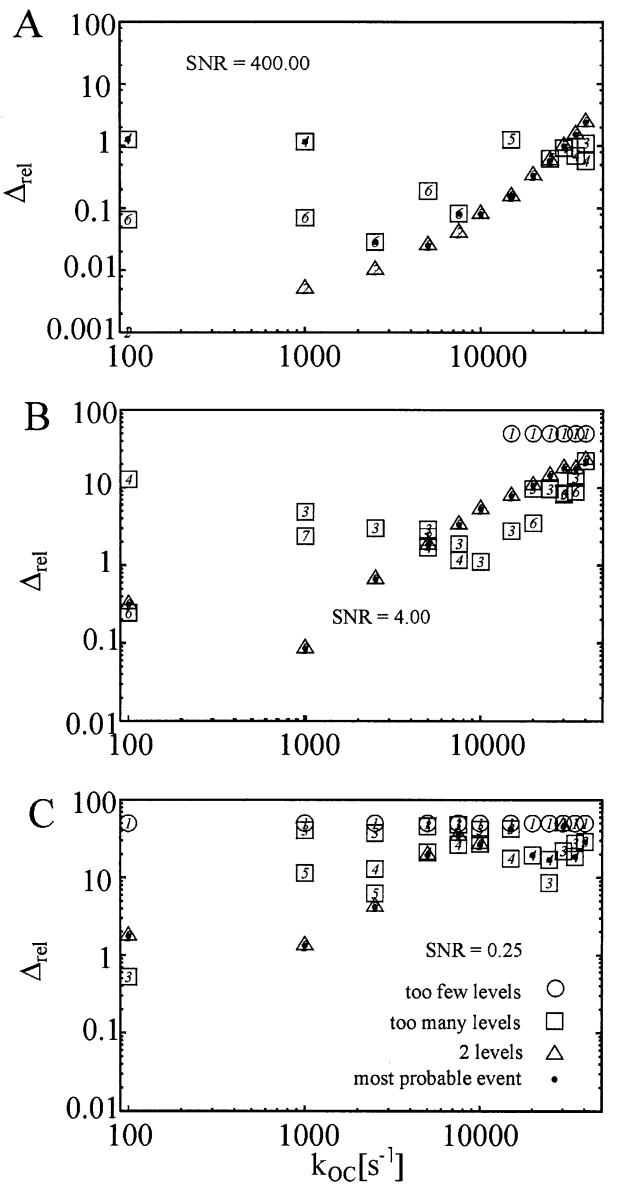


**Fig. 7.** Performance of the level detector for data simulated on the basis of the 2-state model in Fig. 1. (*A*) SNR = 400; (*B*) SNR = 4; (*C*) SNR = 0.25. $k_{OC}$ is given at the bottom abscissa. $\Delta_{rel}$ (in %) is calculated by Eq. 14. The meaning of the symbols is ○ = too few levels, □ = too many levels, Δ = correct number of levels = 2. A dot in the symbol indicates that this solution has minimum scatter $\sigma_\sigma$ (Eq. 13b). A dot in Δ gives the correctly predicted level.

In the following figures, the $k$ (Fig. 1) as a measure of the gating frequency is given on the abscissa, $\Delta_{rel}$ (in %) on the ordinate and the number of levels is presented as parameter by the following symbols: ○ = too few levels, □ = too many levels, Δ = correct number of levels. A dot in the symbol indicates that this solution has minimum scatter $\sigma_\sigma$ (Eq. 13b). A dot in Δ indicates that the correct number of levels has been predicted.

Figure 7 shows the results of simulations obtained from 1 channel of the symmetric 2-state model (Fig. 1, $k_{CO} = k_{OC} = k$). The correct number of levels is found down to an SNR of 0.25, and the relative error $\Delta^2_{rel}$ (in %) stays beyond 10% even at high rate constants. At the highest frequencies, the increasing error $\Delta_{rel}$ is not a failure of the level detector, but an effect of the anti-aliasing filter shifting the apparent level (Hansen et al., 1997). The strange effect is the obvious failure in Fig. 7*A* at 100 and 1000 $sec^{-1}$. Actually, a patcher would not worry, because such a good SNR would never occur. However, these data points are shown in order to demonstrate the effect of bit noise at extreme SNRs that causes additional level jumps with steps quite higher than the $\sigma_{bn}$ of the noise. The nearly parallel behavior of $\Delta_{rel}$ in Fig. 7*A* and *B* shows that not the noise, but the anti-aliasing filter is the origin of $\Delta_{rel}$. At SNR = 0.25 the detector fails beyond 2000 $sec^{-1}$.

The 2-state model with 3 channels (Fig. 8) yields shorter dwell times compared to the 1-channel record with the same rate constants. Nevertheless, the performance of the level detector is still good at SNR = 400 and SNR = 4. Again, the effect of the anti-aliasing filter on the apparent level leads to a parallel behavior in Fig. 8*A* and *B*. However, at SNR = 0.25, the level detector fails. In most cases, the highest level is not found because the detection of its rare occurrence is distorted by noise (dot in the circle, indicating that a lower number of levels was favored by the $\sigma_\sigma$-criterion, Eq. 13b).

The asymmetrical 2-state model with 1 channel is presented in Fig. 9. The rate constant $k_{CO}$ was constant at 16 $sec^{-1}$. $k_{OC} = k$ is shown at the abscissa. The performance is still good at SNR = 0.25 because of the long dwell times related to $k_{CO}$. Again, the high error at high frequencies is not a failure of the level detector, but is caused by the smoothing effect of the anti-aliasing effect as in Figs. 7 and 8.

Another special problem of fast gating is illustrated by means of the 5-state model in Fig. 1. This model with $k = 20$ was used by Farohki et al. (2000) to describe fast gating in *Chara*. Figure 10 shows that the correct number of levels was found for bad SNRs (SNR = 0.25 and SNR = 1), even though the error $\Delta_{rel}$ was between 20 to 30%. Surprisingly, three levels instead of 2 were found at good SNRs. Again, this apparent failure at high gating frequencies even at good SNRs in Fig. 10 does not result from a failure of the level detector. An additional state results from the smoothing effect of the anti-aliasing filter. It averages over bursts of fast gating, and the reduced average current value is delivered as an apparent state to the output of the filter. In the case of low noise, the rare occurrence of bursts with low gating frequencies (from the tail of the dwell-time distributions) is not corrupted by noise. This gives the output of the filter a chance to reach the full level, which sometimes leads to the coexistence of the full and the reduced level, thus increasing the number of apparent levels.

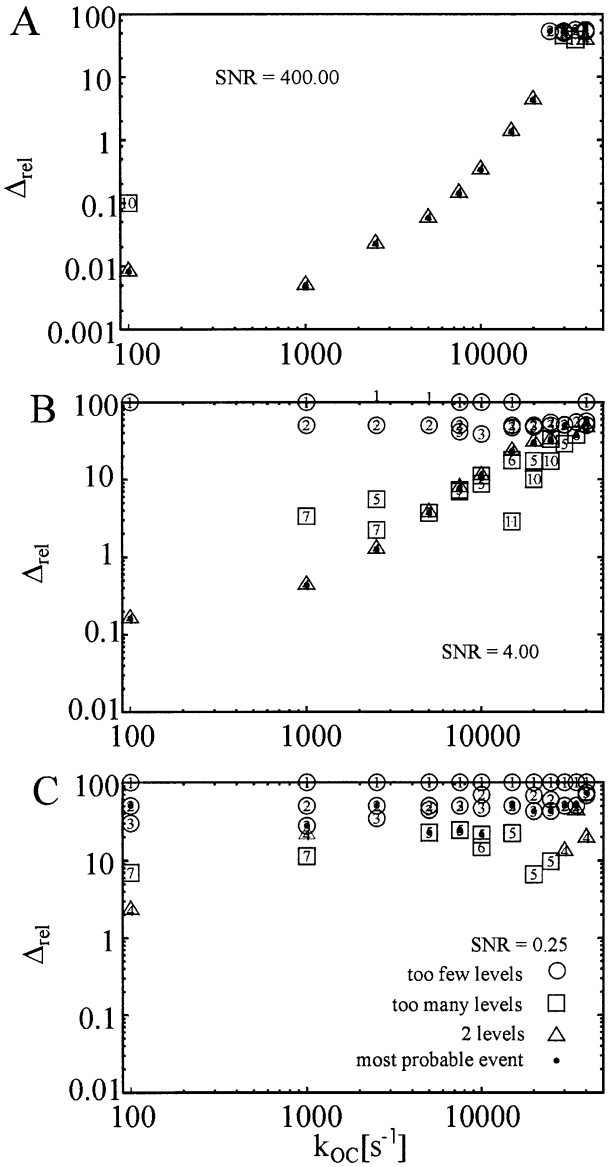


**Fig. 8.** Performance of the level detector for data simulated on the basis of 3 channels of the 2-state model in Fig. 1. (*A*) SNR = 400; (*B*) SNR = 4; (*C*) SNR = 0.25. *k* is given at the bottom abscissa. $\Delta_{rel}$ (in %) is calculated by Eq. 14. The meaning of the symbols is ○ = too few levels, □ = too many levels, Δ = correct number of levels = 4. A dot in the symbol indicates that this solution has minimum scatter $\sigma_S$ (Eq. 13b).

This apparent reduced state resulting from the averaging function of the anti-aliasing filter has been the reason that the AMFE (anomalous mole fraction effect) was considered to result from lower single-channel conductivity and led to the suggestion of the models of Hille and Schwarz (1978) or Wu (1992). However, Farokhi et al. (2000) could show that the stream of ions through the channel is interrupted with a gating frequency of about 100 kHz, leading to a reduced apparent single-channel conductivity at the output of the anti-aliasing filter. This state cannot be

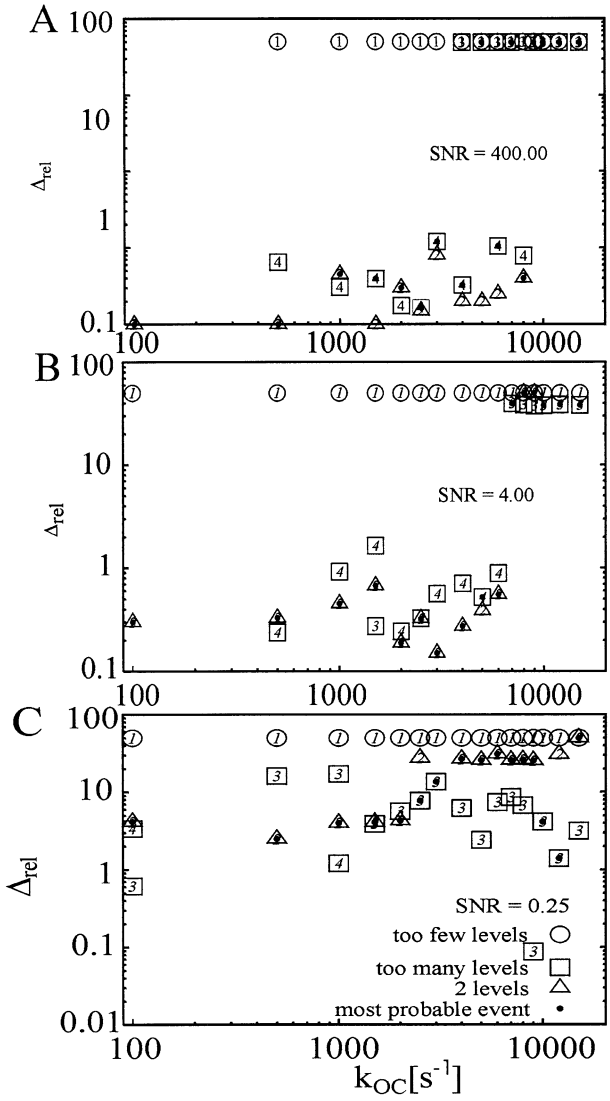


**Fig. 9.** Asymmetrical 2-state model with $k_{CO}$ = 16 $sec^{-1}$, and $k_{OC}$ = *k* given at the abscissa. (*A*) SNR = 400; (*B*) SNR = 4; (*C*) SNR = 0.25.

distinguished from real states by level detectors. In the case of good SNR, this fast gating may become obvious in an asymmetry of the amplitude histograms, as described by beta-distributions (FitzHugh, 1983; Yellen, 1984; Riessner, 1998).

## Comparison of Different Methods of Level Detection

Three different methods were employed for the comparison: the level detector described here, the gauss fit, and the fit-by-eye. The gauss fit approximates the amplitude histogram A(I) of the time series by a sum of Gaussians

$$A(I) = \sum_{i=1}^{m_E} b_i \exp \frac{(S_i - I)^2}{\sigma_i} \qquad (15)$$

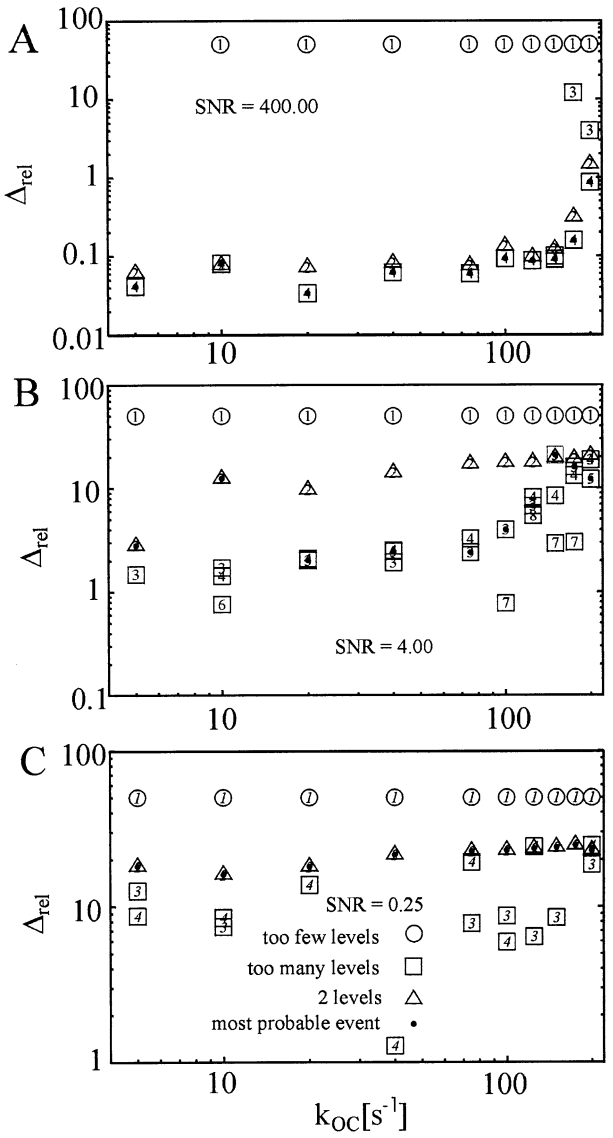


**Fig. 10.** Application of the level detector to the 5-state model in Fig. 1. The failure at good SNR as indicated by the dot in □ in (*A*) results from fast gating.

with $S_i$ being the mean value of the current of Markov level i, $\sigma_i$ the mean value of the noise at that level, and $m_E$ the maximum number of levels.

The fit by eye adjusts the lines on the screen of a computer by means of the cursor keys until the operator gets the impression that they are in the middle of the noisy bands (Fig. 3*B*) related to the selected level.

Table 1 shows the levels and $\Delta_{rel}$ obtained for 3 channels of the 2-state model as used also for Fig. 7. The real $S_i$ are at 1000, 1100, 1200, and 1300. Results from the asymmetrical 2-state model are given in Table 2.

Both tables show that at low frequencies the performance of the level detector is slightly better than the fit-by-eye. At very high frequencies, the fit-by-eye gets better results. The gauss fit seems to do quite well. However, the numbers in Table 1 and Table 2 give a wrong picture with respect to the gaussian fit. Figure 11 shows the amplitude histogram in the case of the 7.5-kHz data in Table 1. It is obvious that the smooth dome in Fig. 11 does not have enough characteristic features to determine 5 to 8 parameters (Eq. 15) by a fitting routine. The gauss fit failed completely when it had to start from arbitrary values. Here it was used for a different purpose. It was given the data from the level detector or from the fit-by-eye, and then it was checked whether these values could still be improved by fitting the amplitude histogram. The tables show that there was no improvement by the gaussian fit.

The problem of overlapping σ-environments is illustrated by the application to real data. A major challenge is the application to a $K^+$ channel in maize channel. Its analysis is difficult because of small single-channel currents, fast flickering and high noise levels (Fig. 12*A*) probably due to bad sealing properties, resulting from the difficulty to cope with the suberin layers of these cells (Keunecke et al, 1997; Keunecke & Hansen, 2000). Averaging of the signal obtained at a sampling rate of 200 kHz and a filter of 50 kHz would smooth out the jumps between levels, and the amplitude histograms do not display peaks (Fig. 12B).

A time series of 2 million data points was split into 3, 4, 5, and 6 parts. For every set of parts, plateaus (Fig. 5) were found for 2, 3, 4 (5) levels. All solutions gave the same ground level (1716 or 1717 digits of the DA-converter that was assigned to 0 pA). The results for 6 parts were [number of levels ($m_E$); average $\sigma_{Si}$ (pA), $\sigma_\sigma$ (pA)]: [2: 0.904, 0.0349]; [3: 1.014, 0.040]; [4: 1.021, 0.014].

According to the $\sigma_\sigma$ criterion of Fig. 6, the solution with 4 levels should be selected. However, other criteria led to a strong preference of the solution with 3 levels over that with 4 levels: (1) The number of putative jump-free sections assigned to the final levels is extremely low for the 4-level solution (7387 sections) compared to the 3-level solution (36552 sections). (2) The 3-level solution was reproduced in all sets with 3, 4, 5, or 6 parts of the time series with levels at 0, 1.65 and 3.3 pA (2 channels of 1.65 pA). The 4-level solution gave different current values for different partitions of the time series. When the whole time series was split into 4 parts, the 4-level solution was replaced by a 5-level solution. The levels of the 4-level solution (with 4 parts of the time series) were at 0, 0.86, 1.7, and 2.9 pA. Thus, they have to be assigned to an unlikely scenario, namely to one channel with 2 sublevels. This results from the fact that the highest level cannot be obtained as a multiple of the lower levels, as would be expected in records containing groups of identical channels. However,

**Table 1.** Levels and $\Delta_{rel}$ (in %) obtained from the evaluation of the symmetrical 2-state model in Fig. 1 with 3 channels by means of three different methods. The real $S_i$ are at 1000, 1100, 1200, and 1300.

| $k_{CO}$ | SNR | Detected levels and errors of the fit | | |
|---|---|---|---|---|
| | | Fit-by-person | Gauss-fit | Level detector |
| 2.5 msec$^{-1}$ | 4 | 1006, 1103, 1200, 1297<br>$\Delta_{rel}$ = 3 | 1006, 1103, 1200, 1297<br>$\Delta_{rel}$ = 3 | 1001, 1101, 1199, 1298<br>$\Delta_{rel}$ = 1.25 |
| 7.5 msec$^{-1}$ | 4 | 990, 1094, 1198, 1302<br>$\Delta_{rel}$ = 5 | 1013, 1105, 1197, 1289<br>$\Delta_{rel}$ = 8 | 1009, 1105, 1193, 1290<br>$\Delta_{rel}$ = 7.75 |
| 25 msec$^{-1}$ | 4 | 1060, 1151, 1242<br>— | 974, 1062, 1150, 1238<br>$\Delta_{rel}$ = 44 | 1049, 1130, 1187, 1262<br>$\Delta_{rel}$ = 32.5 |
| 30 msec$^{-1}$ | 4 | 1047, 1123, 1199, 1275<br>$\Delta_{rel}$ = 24 | 1036, 1113, 1190, 1267<br>$\Delta_{rel}$ = 23 | 1072, 1153, 1221<br>— |

**Table 2.** Levels and $\Delta_{rel}$ (in %) obtained from the evaluation of the asymmetrical 2-state model in Fig. 1 with 1 channel by means of three different methods. The real $S_i$ are at 1000 and 1100.

| $k_{CO}$ | $k_{OC}$ | SNR | Detected levels and errors of the fit | | |
|---|---|---|---|---|---|
| | | | Fit-by-person | Gauss-fit | Level detector |
| 16 sec$^{-1}$ | 2 msec$^{-1}$ | 0.25 | 1016, 1116<br>$\Delta_{rel}$ = 16 | 898, 1104<br>$\Delta_{rel}$ = 53 | 993, 1097<br>$\Delta_{rel}$ = 5 |
| 2 sec$^{-1}$ | 500 sec$^{-1}$ | 0.25 | 1015, 1131<br>$\Delta_{rel}$ = 23 | 891, 1103<br>$\Delta_{rel}$ = 56 | 996, 1089<br>$\Delta_{rel}$ = 7.5 |
| 16 sec$^{-1}$ | 10 msec$^{-1}$ | 9 | 1002, 1104<br>$\Delta_{rel}$ =3 | 1001, 1094<br>$\Delta_{rel}$ = 3.5 | 990, 1006<br>$\Delta_{rel}$ = 52 |

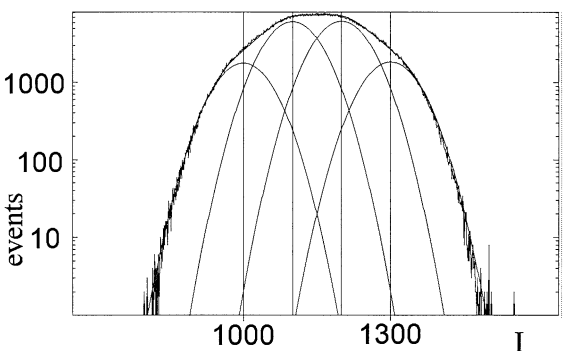


**Fig. 11.** Amplitude histogram of the time series generated by three channels of the symmetrical Markov model used in Fig. 8 and Table 1 with SNR = 4. The smooth lines are the Gaussian distributions of the noise, and the vertical lines give the levels (Eq. 15).

even if such a combination were found, the model test suggested by Caliebe, Rösler & Hansen (2002) should be applied.

The 3-level solution selected by the above four criteria turned out to be identical to that found by Keunecke et al. (1997). The failure of the criterion of Fig. 6 in the case of records with overlapping σ environments results from the following fact. Undetected jumps may lead to false levels between the true levels. Such a false level narrows the distance between levels, and thus it can happen that the false level falls into the range that is tolerated by the Student's *t*-test of Eq. 12. Consequently, most of the sections that have a true mean value will be discarded by the Student's *t*-test level because they can be assigned to two levels. This leads to two effects: Strong decrease of the number of levels that survive, and a shift of the true levels away from the false level, because those sections that are further away from the false level have a higher chance to survive. Both effects are found in the 4-level solution as all levels besides the ground level were different from those of the 3-level solution and from those of the 4- or 5-level solution with other partitions of the time series. Thus, the above considerations turned out to be an adequate replacement for the criterion in Fig. 6. The amplitude histogram (Fig. 12*B*) is no help. All solutions could be fitted to the envelope of the amplitude histogram.

## Conclusions

The failure of the gaussian fits implies that there is only a competition between the fit-by-eye and the automatic level detector. It may be disappointing that at high frequencies the level detector did not give better results than the fit by eye. However, the following features have to be taken into account: Probably the protein computer used for the fit-by-eye makes use of a similar algorithm as the silicon computer used for the level detector. Also, the person who adjusts the horizontal lines in Fig. 11 or Fig.

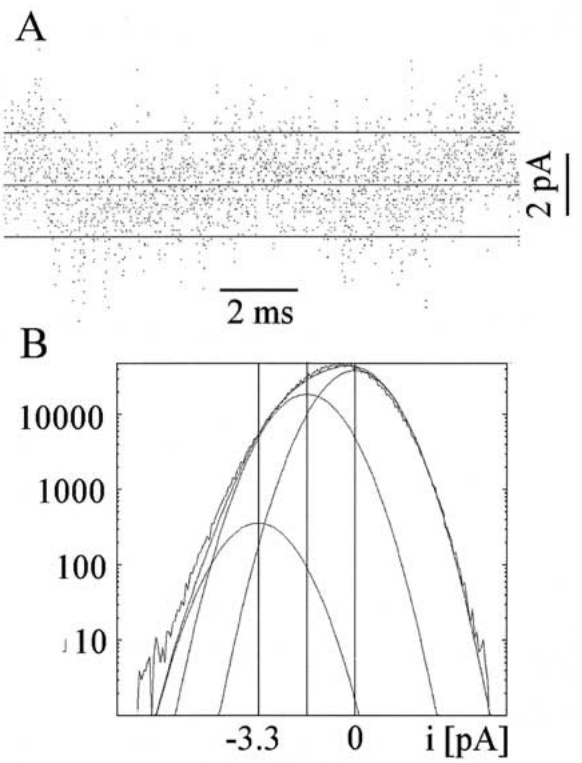


**Fig. 12.** Application of the level detector to real data from a $K^+$ channel in maize. (*A*). The levels of the most likely solution indicated by the horizontal line. (*B*). Amplitude histogram of the time series with the levels taken from (*A*) and the common scatter $\sigma$ as obtained from fitting the histogram. This $\sigma$ (1.01 pA) was about equal to that given by the level detector

12 uses the width of the cloud as a measure of $\sigma_{bn}$ and employs an algorithm similar to the grouping process for the assignment of the jump-free sections. As mammalian protein computers have a superb image-processing software, a some what better performance in time series with fast gating may not be surprising.

On the other hand, the fit-per-eye requires a very experienced person (one out of five in our group), whereas in most cases, the level detector reaches a similar quality without human interference. This may be a great benefit if large amounts of data have to be analyzed, and/or experienced persons are not around.

The work was supported by the Deutsche Forschungsgemeinschaft.

## References

Albertsen, A., Hansen, U.P. 1994. Estimation of kinetic rate constants from multi-channel recordings by a direct fit of the time series. *Biophys. J.* **67:**1393–1403

Ball, F.G., Rice, J.A. 1992. Stochastic models for ion channels: introduction and bibliography. *Math. Biosci.* **112:**189–206

Ball, B.F., Yeo, G.F., Milne, R.K., Edeson, R.O., Madsen, B.W., Sansom, M.S.P. 1993. Single ion channel models incorporating aggregation and time interval omission. *Biophys. J.* **64:**357–367

Bendat, J.S., Piersol, A.G. 1971. Random Data: Analysis and Measurement Procedures. John Wiley & Sons. New York

Blunck, R., Kirst, U., Riessner, T., Hansen, U.P. 1998. How powerful is the dwell-time analysis of multi-channel records? *J. Membrane Biol.* **165:**19–35

Caliebe, A., Rösler, U., Hansen, U.P. 2002. A $\chi^2$ Test for model determination and sublevel detection in ion channel analysis. *J. Membrane Biol.* **185:**25–41

Colquhoun, D., Hawkes, A.G., Srodzinski, K. 1996. Joint distributions of apparent open times and shut times of single ion channels and the maximum likelihood fitting of mechanisms. *Phil. Trans. Roy. Soc. Lond.* A **354:**2555–2590

Crouzy, S.C., Sigworth, F.J. 1990. Yet another approach to the dwell-time omission problem of single-channel analysis. *Biophys. J.* **58:**731–743

Draber, S., Schultze, R. 1994. Detection of jumps in single-channel data containing subconductance levels. *Biophys. J.* **67:**1404–1413

Farokhi, A., Keunecke, M., Hansen, U.P. 2000. The Anomalous Mole Fraction Effect in *Chara*: Gating at the edge of temporal resolution. *Biophys. J.* **79:**3072–3082

FitzHugh, R. 1983. Statistical properties of the asymmetric random telegraph signal with application to single channel analysis. *Math. Biosci.* **64:**75–89

Fredkin, D.R., Rice, J.A. 1992. Maximum likelihood estimation and identification directly from single-channel recordings. *Proc. R. Soc. Lond.* **B 249:**125–132

Hansen, U.P., Albertsen, A, Moldaenke, C., Draber, S., Schultze, R. 1995. Detecting events in signals from sensors: the Hinkley-detector is the answer. *Sensors and Materials* **7:**289–300

Hansen, U.P., Keunecke, M., Blunck, R. 1997. Gating and permeation models of plant channels. *J. Exp. Bot.* **48:**365–382

Hille, B., Schwarz, W. 1978. Potassium channels as multi-ion single-file pores. *J. Gen. Physiol.* **72:**409–442

Horváth, L. 1993. The maximum likelihood method for testing changes in the parameters of normal observations. *Ann. Statist.* **21:**671–680

Horváth, L., Steinebach, J. 2000. Testing for changes in the mean or variance of a stochastic process under weak invariance. *J. Statist. Plann. Inference* **91:**365–376

Hušková, M., Steinebach, J. 2000. Limit theorems for a class of tests of gradual changes. *J. Statist. Plann. Inference* **89:**57–77

Keunecke, M., Hansen, U.P. 2000. Different pH-dependence of $K^+$ channel activity in bundle sheath and mesophyll cells of maize leaves. *Planta* **210:**792–800

Keunecke, M., Sutter, J.U., Sattelmacher, B., Hansen, U.P. 1997. Isolation and patch clamp measurements of xylem contact cells for the study of their role in the exchange between apoplast and symplast of leaves. *Plant Soil* **196:**239–244

Klein, S., Timmer, J., Honerkamp, J. 1997. Analysis of multi channel patch clamp recordings by Hidden Markov models. *Biometrics* **53:**870–884

Klieber, H.-G., Gradmann, D. 1993. Enzyme kinetics of the prime $K^+$ channel in the tonoplast of *Chara*: selectivity and inhibition. *J. Membrane Biol.* **132:**253–265

Korn, S.J., Horn, R.A. 1988. Statistical discrimination of fractal and Markov models of single-channel gating. *Biophys. J.* **54:**871–877

Kreyszig E. 1982. Statistische Methoden und ihre Anwendungen. Vandenhoeck und Ruprecht. Göttingen

Magleby, K.L., Song, L. 1992. Dependency plots suggest the kinetic structure of ion channels. *Proc. Roy. Soc. Lond* **B 249:**133–142

Magleby, K.L., Weiss, D.S. 1990. Identifying kinetic gating mechanisms for ion channels by using two-dimensional distributions of simulated dwell times. *Proc. R. Soc. Lond.* **B 241:**220–228

Patlak J.B. 1993. Measuring kinetics of complex single ion channel data using mean-variance histograms. *Biophys. J.* **65:**29–42

Press, W.H., Flannery, B.P., Teukolsky, S.A., Vetterling, W.T. 1987. Numerical Recipes. The Art of Scientific Computing. Cambridge University Press, Cambridge, New York, New Rochelle, Melbourne, Sidney

Riessner T. 1998. Level Detection and Extended Beta Distributions for the Analysis of Fast Rate Constants of Markov Processes in Sampled Data. Shaker Verlag, Aachen

Schultze, R., Draber, S. 1993. A nonlinear filter algorithm for detection of jumps in patch clamp data. *J. Membrane Biol.* **132:**41–52

Townsend, C., Horn, R. 1999. Interaction between the pore and the fast gate of the cardiac sodium channel. *J. Gen. Physiol.* **113:**321–331

Wu, J. 1992. Dynamic ion-ion and water-ion interactions in ion channels. *Biophys. J.* **61:**1316–1331

Yellen, G. 1984. Ionic permeation and blockade in $Ca^{2+}$ activated $K^{+}$ channels of bovine chromaffin cells. *J. Gen. Physiol.* **84:**157–186

Yeo, G.F., Milne, R.K. Edeson, R.O., Madsen, B.W. 1988. Stastistical inference from single channel records: two state Markov model with limited time resolution. *Proc. R. Soc. Lond.* **B 235:**63–94

Zheng, J., Vankataramanan, L., Sigworth, F.J. 2001. Hidden Markov model analysis of intermediate gating steps associated with the pore gate of Shaker potassium channels. *J. Gen. Physiol.* **118:**547–562